Pattern Formation and Morphology Evolution in Langmuir Monolayers

A. Flores,[†] E. Corvera-Poiré,[‡] C. Garza,[†] and R. Castillo*,[†]

Instituto de Física, UNAM, P. O. Box 20-364, D. F. 01000, México, and Facultad de Química, UNAM, Cd. Universitaria, D. F. 45010, México

We present a study of how patterns formed by Langmuir monolayer domains of a stable phase, usually solid or liquid condensed, propagate into a metastable one, usually liquid expanded. During this propagation, the interface between the two phases moves as the metastable phase is transformed into the more stable one. The interface becomes unstable and forms patterns as a result of the competition between a chemical potential gradient that destabilizes the interface on one hand and line tension that stabilizes the interface on the other. During domain growth, we found a morphology transition from tip splitting to side branching; doublons were also found. These morphological features were observed with Brewster angle microscopy in three different monolayers at the water/air interface: dioctadecylamine, ethyl palmitate, and ethyl stearate. In addition, we observed the onset of the instability in round domains when an abrupt lateral pressure jump is made on the monolayer. Frequency histograms of unstable wavelengths are consistent with the linear-instability dispersion relation of classical free-boundary models. For the case of dendritic morphologies, we measured the radius of the dendrite tip as a function of the dendrite length as well as the spacing of the side branches along a dendrite. Finally, a possible explanation of why Langmuir monolayers present this kind of nonequilibrium growth patterns is presented. In the steady state, the growth behavior is determined by Laplace's equation in the particle density with specific boundary conditions. These equations are equivalent to those used in the theory of morphology diagrams for two-dimensional diffusional growth, where morphological transitions of the kind observed here have been predicted.

1. Introduction

Amphiphilic molecules that are nearly insoluble in water can form Langmuir monolayers (LMs) at the air/water interface. The most common way to study LMs has been through measurements of the pressure−area isotherms, $\Pi(A,T) = \gamma_0(T) - \gamma(A,T)$, where T is the temperature, A is the area per molecule, and γ and γ_0 are the surface tensions of the monolayer and of pure water, respectively. In the last 15 years, new experimental techniques have revealed that many of the singularities observed in surface pressure−area isotherms since the works of Stenhagen[1] and Ludquist[2,3] are due to phase changes, where each phase can be described in terms of four order parameters.[4,5] Grazing incidence X-ray diffraction gives the most explicit information about monolayer order.[6] Nevertheless, it is not practical for studying the dynamics of phase transitions. Other powerful techniques have been developed to study monolayer organization, such as polarized fluorescence microscopy[7] and Brewster angle microscopy[8,9] (BAM). These techniques complement the information given by X-ray experiments, because they survey larger scales ($\sim$200 μm), providing information about homogeneity, texture, structure, and dynamics. In particular, BAM is a noninvasive optical technique quite sensible for observing very fine details during phase transformations, and it is probably the best suited to be used in direct observations during compression or expansion of monolayers.

In this paper, we present a study of how patterns formed by monolayer domains of a stable phase, usually solid or liquid condensed, propagate into a metastable one, usually liquid expanded. During this propagation, the interface between the two phases moves as the metastable phase is transformed into the more stable one. The interface becomes unstable and forms patterns because of the competition between a chemical potential gradient that destabilizes the interface on one hand and line tension that stabilizes the interface on the other. The further the system is out of equilibrium, the faster the metastable phase will turn into the stabler phase and, consequently, the faster the interface will propagate. The competition between effects that stabilize and destabilize the system gives rise to characteristic length scales of growing domains and determines, together with the anisotropy, the overall shape and symmetry of domain patterns. The balance between competing effects varies as the growth conditions change. The observed patterns may be grouped into a small number of typical patterns or morphologies, each representing a different dominant effect. Here, we will focus on tip-splitting growth, which gives rise to dense branched morphologies called seaweeds, and on dendritic growth, which is characterized by side branching. For a given system, each morphology is observed over a range of growth conditions, bringing to mind the idea of a morphology diagram and the existence of a morphology selection principle. This one would select a particular morphology and, consequently, the corresponding transitions, as we vary the growth conditions. In equilibrium, the phase that minimizes the free energy is selected and observed. The existence of an equivalent principle for out-of-equilibrium systems is one of the longest pursued and yet unsolved questions in the study of pattern formation.

In LMs made of a single component, the problem of nonequilibrium growth morphologies is subtler than that in

---

* To whom correspondence should be addressed.
[†] Instituto de Física.
[‡] Facultad de Química.

Pattern Formation and Morphology Evolution in LMs

J. Phys. Chem. B, Vol. 110, No. 10, 2006 **4825**

three-dimensional (3D) solids. In the latter case, the heat released during the phase transition has to be diffused far away from the interface before the front can advance further. In LMs, this mechanism can be ruled out because the monolayer rests on a large body of water (subphase) that acts as an isothermal reservoir, absorbing all of the latent heat released during the phase transition. In monolayers, growing instabilities are usually observed along a fluid/nonfluid phase transition (LE/LC, LE/S), where the involved phases have a large difference in area density (~50%); amphiphiles usually have some kind of hindrance (two or more tails, a chiral center, bent tails due to double bonds, etc.). Supersaturation induces domain growth, which, depending on the experimental conditions, forms fractal, seaweed, and dendritic morphologies. Therefore, just as in 3D systems, the important questions in LMs are the following: Why does such a complex morphology evolve in uniform environments? Why do we not simply observe circular 2D domains? How are length scales selected as tip radius, width, and spacing of the side braches? Why does the morphology of a growing domain change from tip splitting to side branching?

The questions listed above have given to the area of pattern formation around 30 years of development, but as far as we know, even the experimental observations leading to the questions just made above have not been discussed for LMs. This is the topic under discussion in this paper. We present how, at some point during the domain growth, there is a morphology transition from tip splitting to side branching. This is observed for three different monolayers at the air/water interface using BAM: dioctadecylamine (DODA), ethyl palmitate (EP), and ethyl stearate (ES). In the case of dendritic morphology, we measured the radius of the dendrite tip versus the dendrite length as well as the spacing of the side branches along a dendrite. In addition, we prepared experiments to show how the instability starts at round domains when an abrupt lateral pressure jump is made on the monolayer; frequency-versus-periodicity diagrams for the instability are consistent with the dispersion relation given in classical free-boundary models. Doublons are observed, and atomic force microscopy (AFM) observations of Langmuir–Blodgett (LB) transferred monolayers on mica are presented. At the end of the paper, an explanation that allows us to understand our observations is presented. In the steady state, the growth behavior is determined by Laplace's equation in the particle density with specific boundary conditions. These equations are equivalent to those used in the theory of morphology for 2D diffusional growth, where morphological transitions of the kind presented here have been predicted by Müller-Krumbhaar and collaborators.[10-15]

A. Liquid–Solid Phase Transitions in 3D. Pattern formation in 3D has a long history.[16] In the late 1940s, Ivantsov[17] studied the problem of solidification from an undercooled melt with a model that ignored interfacial effects. He found that, for any value of the undercooling, Δ, there exists a continuous family of steady-state solutions all with parabolic shape, where the product of the tip radius, R_o, and the growth velocity for each parabola, V, was a constant ($R_o V = f(\Delta)$); that is, Ivantsov's solution specified such a product, but it could not predict either of the quantities alone, suggesting that dendrites with different tip curvatures and corresponding tip velocities coexist, at a specified undercooling. However, it was experimentally demonstrated that, under controlled conditions, for a given undercooling, the same dendrite is reproducible, implying a selection problem.[18] Mullins and Sekerka[19] showed that, in addition to the above difficulty, Ivantsov's solutions were linearly unstable, so none of them could be observed. The first attempts to solve
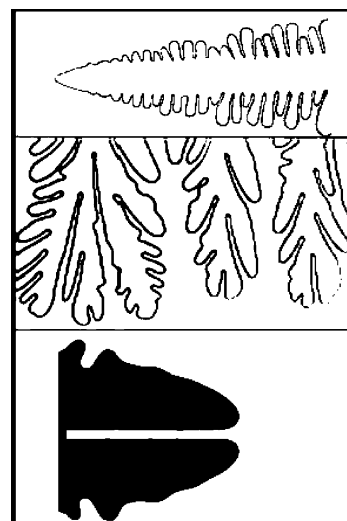

Figure 1. Morphologies: (upper panel) dendrite growing from right to left, with its characteristic needle tip and side branches (adapted from Figure 1 of ref 69); (medium panel) seaweeds growing downward with their typical tip splitting (adapted from Figure 17 of ref 15); (lower panel) 2D doublon with its typical inner groove along the axis of symmetry between two fingers (adapted from Figure 2 of ref 48).

the selection problem were based on the assumption that incorporation of surface tension would stabilize the parabolas, while involving only minor shape corrections to Ivantsov's parabolic fronts. This introduced an additional length scale, d_0, the capillary length, that is proportional to surface tension into the problem.[20] Although, it seemed as if the selection problem had been solved, this was not so; different substances that according to predictions would produce similar dendrites by no means did it. In addition, the decoration of a needle crystal with side branches (see Figure 1, top), that is, a dendrite, did not seem to influence the selected velocity dramatically, so the selection problem for the needle crystal included the one for dendrites. The selection problem for growing needle crystals was solved through the microsolvability theory, with the conclusion that surface tension and surface kinetics, despite their small size, turned out to be singular perturbations to the problem that totally change the character of interfacial dynamics.[21,22] When surface tension and surface kinetics are isotropic, dendritic growth does not occur, but rather fingers with tip-splitting dynamics (see Figure 1, middle). Anisotropy is required in the interfacial dynamics to produce dendritic growth.[21] A theory of pattern formation for diffusional growth was developed by Müller-Krumbhaar and co-workers, who were able to develop a morphology diagram,[10-15] where the building block of the dendritic structure is a dendrite with a parabolic tip and the basic element of the seaweed structure is a doublon;[14,15] this is a local structure consisting of two broken-symmetry fingers that are mirror images of each other and separated by a narrow groove of liquid of constant width (see Figure 1, bottom). The control parameters in the morphology diagram are the anisotropy, ϵ, of the capillary length and the undercooling, Δ, and the predicted structures are classified according to whether they are compact or fractal and whether they possess orientational order or not.

Models for the solidification problem have been developed that replace the full diffusion problem in 2D by equations of motion for the interface.[23,24] Recently, the development of the phase-field methods has allowed increasing progress in simulating solidification.[25] Examples of simulation studies for dendritic growth can be seen in refs 25–32. In particular, Provatas et

al.,[30] using a phase-field model for directional solidification, observed a crossover transition from seaweed to dendritic morphology, as the thermal gradient is lowered, for small surface tension anisotropy directed at 45° relative to the pulling direction.

Diffusion limited aggregation (DLA)[33,34] is the most dramatic diffusion instability, where a rule dictating how a single atom is added to an existing cluster of atoms causes the cluster to grow by one particle at a time. Regular DLA does not have analogues to surface tension and to anisotropy, and undercooling does not play a role. However, there have been extensions of this method, replacing the single walker by many walkers, thus performing Monte Carlo simulations of finite Δ[35,36] or incorporating microscopic dynamics via phenomenological rules for sticking probabilities of walkers to the aggregate.[37] In particular, simulations with surface tension lead to branching aggregates with branches of finite width.[38] Although DLA can be seen as a kind of Laplacian growth,[39] it was speculated by many authors[40−42] that both problems belong to the same universality class, and it was expected that the resulting fractal patterns will have the same fractal dimension. Quite recently, some authors[43,44] have shown that there are deep differences between both problems, and these seem to be related to the form of growth. They claim that the key point is that Laplacian patterns are grown layer by layer, whereas DLA is grown particle by particle. Up to date, there is no clear consensus about this issue.

Since the pioneering work of Glicksman,[18] many experiments have been performed to understand the solidification problem. Recent examples can be mentioned: the dendritic and seaweed growth as a function of crystal orientation planes in thin films of the mixture CBr_4/C_2Cl_6,[45] the study of the structure and dynamics of the shape of the tip of xenon dendrites,[46] the directional solidification in succinonitrile alloys that grow differently depending on the growth direction (dendrite along the {100} direction and seaweed near the {111} plane),[47] and the observation of morphology transitions from dendrites to seaweeds in xenon 3D crystals.[48,49] Similar morphology transitions have been observed in thin films of isotactic polystyrene[50] and thin films of poly(ethylene oxide).[50,51]

B. Patterns in Langmuir Monolayers. 2D monolayers display domain patterns in equilibrium.[52−54] The phenomenology of these patterns and of the shapes of their constituent domains can be interpreted as a manifestation of modulated phases,[55] where the periodic spatial organization of a pertinent order parameter is attributed to the presence of competing interactions favoring spatial inhomogeneities in an otherwise uniform phase. Our main interest in this paper is not in equilibrium patterns.

In the literature, experimental studies of patterns formed by monolayer domains when a stable phase is propagating into a metastable one are not common. As far as we know, the first study was of Miller and Möhwald in 1987.[56] They worked with a phospholipid monolayer and explained their observations in terms of a 2D diffusion model with impurities, since they used a dye to observe the monolayer with polarized fluorescence microscopy. In this study, the authors did not recognize the difference between dendritic and seaweed growth; actually, they observed the latter. Using the same observational technique, Rondelez and collaborators[57] conducted the first study on dendritic growth in a chiral amphiphile, D-myristoyl alanine. They obtained that R_o^2V is a constant, as needed by the microsolvability theory. In recent years, monolayer observations have been made with noninvasive BAM. Vollhardt and collaborators reported a variety of nonequilibrium growth structures for monolayers of fatty acid ethyl esters (palmitate and stear-

ate)[58] and 1-monopalmitoyl-*rac*-glycerol[59] using different compression rates; in particular, they observed domains with the tip split. Iimura et al.[60] showed dendritic growth for cis-unsaturated fatty acids. Flores et al.[61] observed dendritic growth in DODA monolayers caused by supersaturation, due to the low incorporation rate of molecules into the condensed phase compared to the rate of molecular area reduction during compression. Chiral effects on the shape of domains for different enantiomeric and racemic mixtures of phospholipids[62−65] and *N*-acyl amino acids[66] have been studied. In these cases, anisotropy in line tension is playing an important role. From the theoretical point of view, a description for the growth of a condensed phase at the expense of an expanded phase with impurities that are also miscible in the subphase has been presented.[67] Bruinsma et al.[68] have also proposed a hydrodynamic mechanism, not experimentally tested yet, based on the Marangoni flow to describe growth instabilities of domains in monolayers.

2. Experimental Section

Amphiphiles. Dioctadecylamine (DODA), $2C_{18}NH$ (≥99%), was purchased from Fluka Chemie (Switzerland). Ethyl stearate (ES) (99%) and ethyl palmitate (EP) (≥99%) were obtained from Sigma-Aldrich Inc. (MO). All of them were used without any further purification.

Monolayers. Amphiphiles were spread onto a subphase of ultrapure water (Nanopure-UV, 18.3 MΩ) in a Langmuir trough. The spreading solution was made with chloroform (Aldrich, U.S.A., HPLC) for DODA and heptane (Aldrich, U.S.A., ≥99%) for ES and EP, in both cases at a concentration of 1 mg/mL. The DODA monolayer subphase was modified with H_2SO_4 (Merck, Mexico) to reach pH 3.[61] The other monolayers were worked at pH 5.5. On many occasions, we modified the subphase viscosity by adding glycerol (≥99.5%) from Sigma-Aldrich Inc. (MO). When the subphase glycerol concentration was up to 10 vol %, the dynamics of domain growth was sensibly slowed, without an appreciable change in the isotherms or in the phase transition texture.

Troughs. Two Nima LB troughs (models TKB 2410A and 601 BAM, Nima Technology Ltd., England) were used. One was devoted to making isotherms and for observing the LMs, and another trough, to developing the Langmuir−Blodgett (LB) films. In both cases, a Wilhelmy plate was used to measure $\Pi(A,T)$ and temperature was kept constant with the aid of a water circulator bath (Cole-Parmer 1268-24, U.S.A.). All experiments were carried out in a clean-room lab.

The trough used to observe the domain growth is a rectangular one. It is made of PTFE with a working area starting at 490 cm^2, and it is isolated from vibrations with a vibration isolation system (model 2S, Halcyonics GmbH, Germany). This trough was put inside of a 1 m^3 plastic box to avoid undesired air convection. The temperature difference between the surroundings defined by the air inside the box and the trough was at most 1 °C. The trough used to develop the LB films was isolated from vibrations using a pneumatic tube incorporated into a steel base. The barriers are made of poly-tetra-fluoro-ethylene or Teflon (PTFE) fitted with stiffening bars defining a working circular area, starting at 1000 cm^2.

BAM. The growth of domains was observed with an Elli2000 imaging ellipsometer (Nanofilm Technologie GmbH, Germany) in the BAM mode (spatial resolution of ∼2 and ∼1 μm using the 10× and 20× objectives, respectively). When the monolayer moved slowly, this instrument allowed us to get observations with the whole field of view in focus, due to its movable objective lens. When this was not the case, we recorded the

Pattern Formation and Morphology Evolution in LMs

J. Phys. Chem. B, Vol. 110, No. 10, 2006 **4827**

observations with a VCR, with a horizontal stripe in focus. BAM observations during the development of the LB films were performed with a BAM1 plus instrument (Nanofilm Technologie GmbH, Germany) with a spatial resolution of ~4 μm.

AFM. LB transferred monolayers were scanned with a scanning probe microscope (JSTM-4200 JEOL, Japan) with a 25 μm × 25 μm scanner. Intermittent contact and phase lag modes were used to obtain topographic and phase images. Noncontact silicon cantilevers with a typical force constant of 40 N m^{-1} (Mickomash, OR) were used.

3. Results and Discussion

Here, we present the results of several experiments addressed to observe the morphology transition from tip splitting to side branching as well as to obtain some length measurements on domains of three monolayers: DODA, EP, and ES; these ones were prepared according to the procedures presented in the Experimental Section. In addition, we present how the instability starts at round domains when an abrupt lateral pressure jump is made on a LM. At the end of this section, we will present an explanation which could help one to understand the morphological features of our observations in monolayers.

A. Morphology Transition. Figure 2 presents BAM images showing different locations of the DODA monolayer ($T = 23.9$ °C), along its evolution after a sudden compression from a vanishing lateral pressure up to $\Pi = 5$ mN/m. Here, we crossed the LE/S_1 phase transition, leaving the LE phase metastable.[61] The growth evolution of domains was observed by maintaining constant the lateral pressure with the aid of the servomechanism of the trough. The long relaxation times of this particular monolayer allowed us to observe the evolution of domains, which would be impossible in other more labile monolayers. It is important to note that monolayers are steadily moving across the observation field of the microscope, because of the induced fluxes created by the domain growth. Thus, our images are observations at different locations along the monolayer as time elapses. At the very beginning, there are small, deformed, round domains that are difficult to see (not shown), because their size is close to the resolution limit of the BAM. Domains continue their growth due to supersaturation and go through a stage where domains grow with a seaweedlike structure (Figure 2a and b); tip splitting is clearly observable. After some time, there is a transition stage where domains grow and show both tip splitting and needle tips in the same domains (Figure 2b and c). Afterward, dendritic growth is clearly observed (Figure 2d−f). In later events, dendrites become thicker (Figure 2f and g), and finally, Ostwald ripening is observed (Figure 2h). Here, the larger domains become even larger and the small ones become smaller or slimmer.

To observe in further detail the morphological domain growth of the S_1 phase in the DODA monolayer, we performed several experiments where the monolayer was compressed up to the phase transition, where LE and S_1 are in coexistence. After a few minutes of relaxation (~15 min), a pressure jump was made by a sudden compression of the monolayer to supersaturate the system. This sudden compression created the equivalent of an undercooling in classical solidification. The pressure reached after the jump was maintained constant. These jumps were repeated several times consecutively to increase the supersaturation level at each jump. After the initial jump, the domains usually were very small, and the smaller ones melted again during the observation time. At larger saturations (second or third pressure jump), the size of the domains allowed for a clear observation of them. Further jumps were in general useless, since
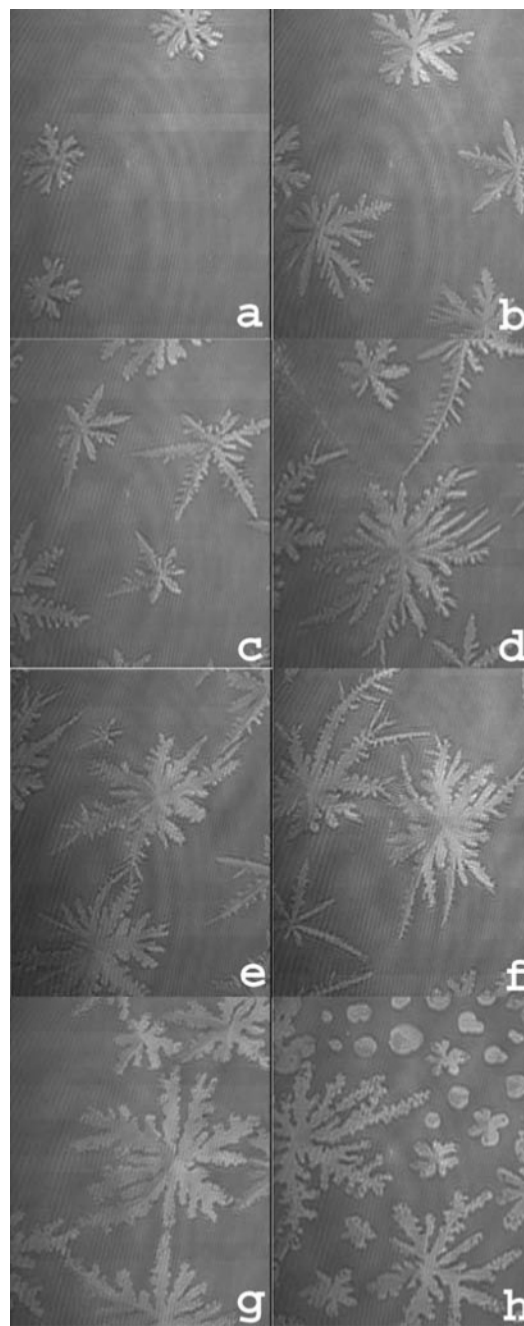
Figure 2. BAM images showing the domain growth of the S_1 phase in the DODA monolayer as time elapses at constant lateral pressure ($\Pi = 5$ mN/m), at $T = 23.9$ °C. The monolayer was suddenly compressed from a vanishing lateral pressure up to $\Pi = 5$ mN/m. Elapsed time: (a) 1 min; (b) 1 min 20 s; (c) 4 min; (d) 6 min; (e) 9 min; (f) 11 min; (g) 2 h 26 min; (h) 2 h 55 min. The horizontal full width is 220 μm for each individual image.

domains became thick and big enough to interact among them. Here, we present three examples for jumps of $\Delta\Pi = 1$, $\Delta\Pi = 2$, and $\Delta\Pi = 4$ mN/m. First, we will present the results for each case, and afterward, a comparison among them will be made.

Figure 3 shows a typical pressure-versus-area graph during an experiment where several sudden compressions produced pressure jumps of $\Delta\Pi = 1$ mN/m, and Figure 4 shows the corresponding BAM images of the monolayer ($T = 24.2$ °C) after the third jump of $\Delta\Pi = 1$ mN/m, that is, at a pressure of $\Pi = 9$ mN/m. At the beginning, flowerlike domains are formed with five to seven leaves, which are not very symmetric, and
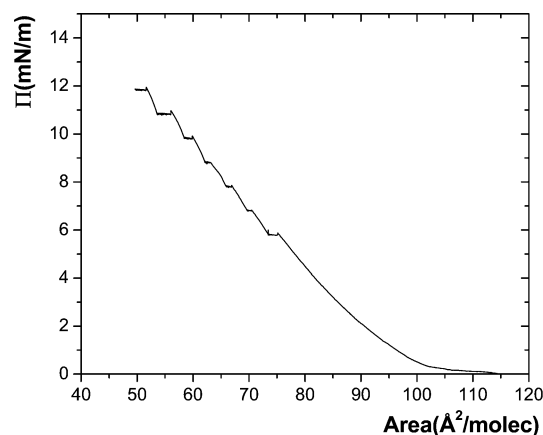
Figure 3. Graph showing lateral pressure vs area during one typical experiment, where several compressions producing pressure jumps of $\Delta\Pi = 1$ mN/m were exerted on the monolayer. Coexistence was at $\Pi \sim 6$ mN/m, i.e., the first plateau. $T = 24.2$ °C.
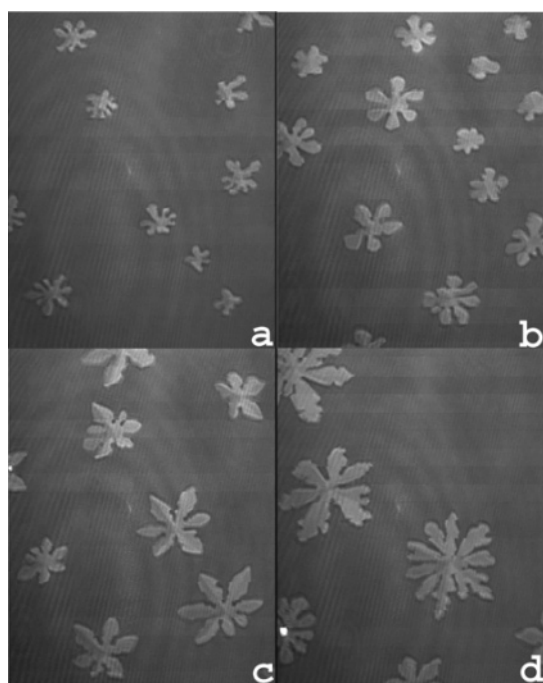

Figure 4. BAM images of the DODA monolayer ($T = 24.2$ °C) after jumps of $\Delta\Pi = 1$ mN/m that reach a final pressure of $\Pi = 9$ mN/m (Elapsed time since jump: a: 68 s, b: 227 s, c: 352 s, d: 503 s). The horizontal full width is 220 μm for each individual image.

most of the time, the leaves are bulged at the ends and some of them show tip splitting (Figure 4a and b). Thereafter, domains grow, on average, with seaweedlike structure caused by the typical tip-splitting dynamics (Figure 4d). However, since the local growing conditions along the trough are surely not exactly the same, it is normal to observe some locations along the monolayer with domains showing tip splitting and others showing thick arrow shaped tips or mixed domains (Figure 4c). Figure 5 shows BAM images of the DODA monolayer ($T = 23.6$ °C) after pressure jumps of $\Delta\Pi = 2$ mN/m that reached a final pressure of $\Pi = 8$ mN/m (second jump). At this saturation level, the monolayer seems to cross a transition zone, growing with dynamics for which tip-splitting and side-branching morphologies were equally likely. Depending on the observed location in the monolayer, we could observe seaweed structures or dendrites, although the later ones were not well formed. It was very common to observe mixed domains, that is, domains with some legs showing tip splitting and some legs showing
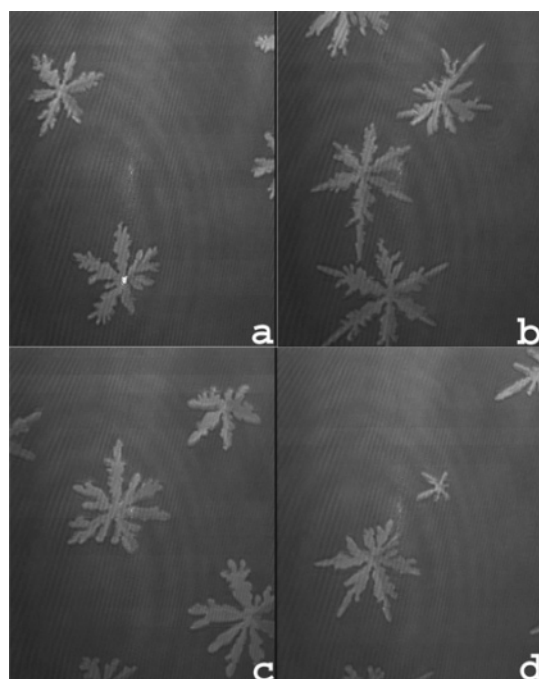

Figure 5. BAM images of the DODA monolayer ($T = 23.6$ °C) after pressure jumps of $\Delta\Pi = 2$ mN/m that reach a final pressure of $\Pi = 8$ mN/m (Elapsed time since jump: a: 32 s, b: 257 s, c: 706 s, d: 811 s). The horizontal full width is 220 μm for each individual image.
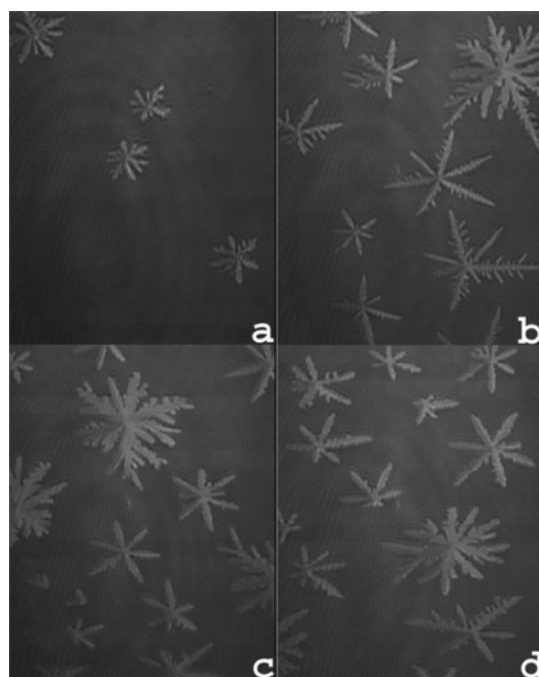

Figure 6. BAM images of the DODA monolayer ($T = 23.5$ °C), with a pressure jump of $\Delta\Pi = 4$ mN/m, that reached a final pressure of $\Pi = 8$ mN/m (Elapsed time since jump: a: 20 s, b: 130 s, c: 552 s, d: 925 s). The horizontal full width is 220 μm for each individual image.

needle tips, with the latter case even showing side branches (usually the larger ones). Figure 5d shows needles growing from the center of former tips that originally were split. Figure 6 shows BAM images of the DODA monolayer ($T = 23.5$ °C) after a pressure jump of $\Delta\Pi = 4$ mN/m that reached a final pressure of $\Pi = 8$ mN/m (after the first jump). Here, the supersaturation was larger than that in the two preceding examples. In this case, even though, at the very beginning, there were some domains showing tip splitting and some deformed
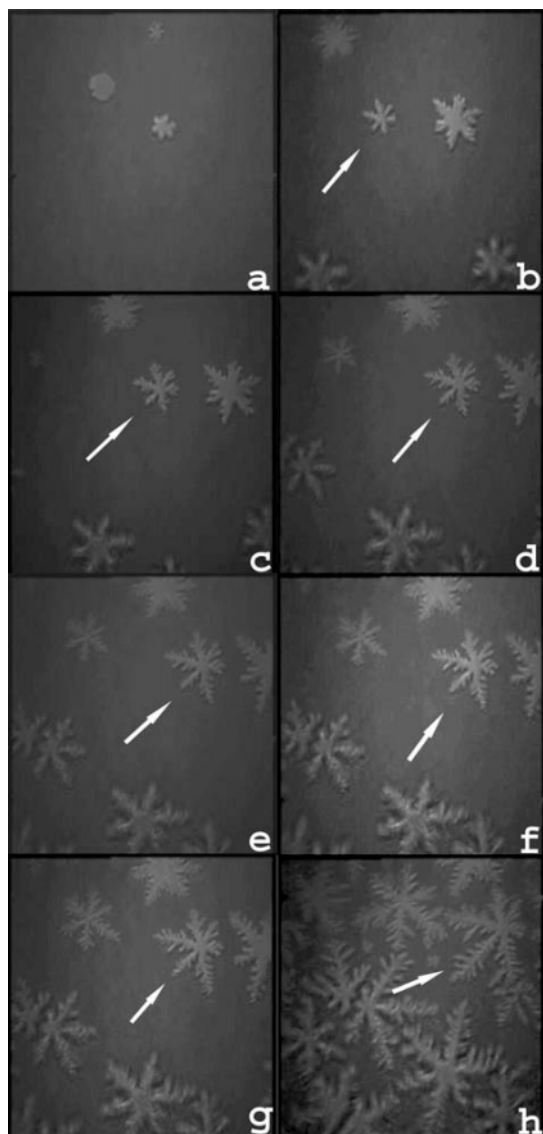
Pattern Formation and Morphology Evolution in LMs

J. Phys. Chem. B, Vol. 110, No. 10, 2006 **4829**

Figure 7. BAM images showing the ethyl stearate L'_2 phase growing into the LE phase at relatively high speed. The monolayer was compressed at 80 cm²/min, at $T = 32$ °C, and the subphase is water/glycerol (10 vol %). The horizontal full width is 430 μm for each individual image. The elapsed time between the first and the last image is 7.5 s. The arrows indicate how a particular domain is growing.

seaweeds turning into dendrites, it was more common to observe domains with six dendritic legs with clear side branching. Finally, a global observation of Figures 4−6, where the essential difference is just the size of the pressure jumps that leads to different supersaturation levels (temperature is almost the same), makes it clear that, at low supersaturation levels, seaweed growth is preferred. On the contrary, at large supersaturation levels, dendritic growth is preferred.

In Figure 7, we present some BAM images coming from a VCR film from a different kind of experiment. Here, the ES monolayer was compressed at relatively high speed (80 cm²/min, at $T = 32$ °C). The images show the L'_2 phase[3] growing into the LE phase. In this case, we added glycerol to the subphase (glycerol 10 vol % in water) to slow the dynamics of domain growth. Here, it was possible to catch the growth of domains just from the beginning, from nearly round domains up to dendritic domains. At the very beginning, there are small round domains and the instability deforms the 1D interface and forms fingers; some of the fingers grow faster and form flowerlike domains. In the next stage, the fingers turn into legs
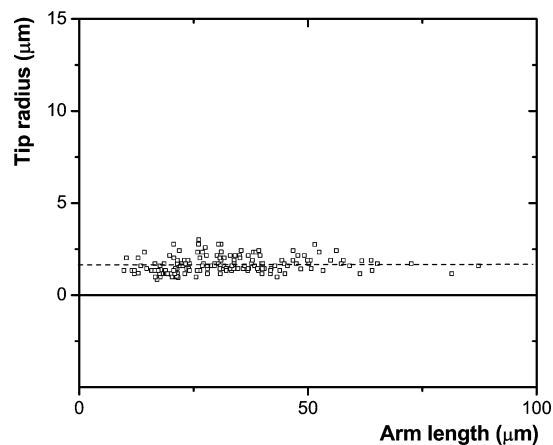

Figure 8. Tip radius vs dendrite length for dendrites in 29 domains developed in a single experiment at $\Pi = 4.5$ mN/m after a pressure jump of 4 mN/m ($T = 22.4$ °C).

that show tip splitting. In the next events, growth is very rapid, and since the local conditions are slightly different along the monolayer, domains show mixed growing dynamics; that is, parts of a domain grow through tip splitting and other parts present needles, which quickly show side branching. At the end, before domains collide, the legs present a clear dendritic morphology (part of the film can be seen in http://www.fisica.unam.mx/liquids/movies/movies.html). The EP monolayer shows exactly the same pattern.

The experiments just presented above clearly show that there is a morphology transition during domain growth of a condensed phase into the metastable fluid LE phase. As far as we know, this has not been observed in LMs. Although, there is a previous work where tip splitting and dendrite formation was discussed.[59]

B. Typical Length Scales. In this section, we present some measurements on our 2D dendritic domains and show that they have similar characteristics as their 3D counterparts. In particular, when dendritic growth was dominant, we measured the dendrite tip radius as a function of dendrite length. This was done on electronic images coming from a Brewster angle microscope, using the Image J software (National Institute of Health, U.S.A., resolution better than 0.16 μm in our images). We fit a circle to the tip of fully developed dendritic legs and measured the distance from that tip to the domain center to which the dendritic legs were attached. Figure 8 is an example showing tip radius versus dendrite length for 29 dendrites of DODA developed in a single experiment at $\Pi = 4.5$ mN/m, after a pressure jump of 4 mN/m at $T = 22.4$ °C. As we can see here, the tip radius is almost insensitive to the dendrite length, probably revealing that the supersaturation level is similar for all dendrites, as well as to the level of anisotropy; thus, there is a selected tip radius.[11] For all measured dendrites, the tip radius was around 1.5 μm depending on the experimental conditions; in the particular case of Figure 8, the average tip radius was 1.7 μm. Our results here are just an estimate, since we are relatively close to the resolution limit of the BAM technique which is 1 μm.

We also measured the periodicity of side branches in dendritic domains. We numbered the side branches at the right and left sides along the main dendritic legs of several domains, starting at the domain center. The position of the side branches was measured from the domain center using the Image J software. An example can be seen in Figure 9, where we show the position for the numbered right side branches (filled symbols) and for the numbered left side branches (open symbols), for eight dendritic arms of the DODA monolayer developed in an
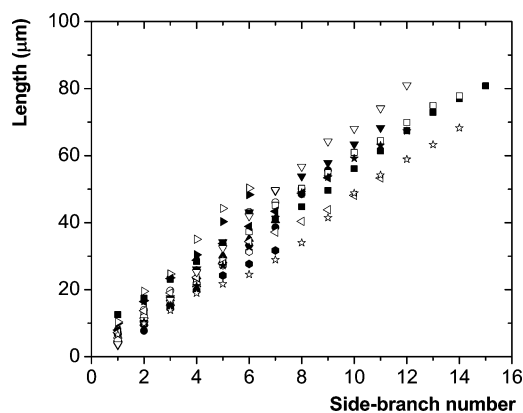
Figure 9. Positions of side branches for eight dendritic arms of the DODA monolayer developed in an experiment ($T = 22.4$ °C) after a pressure jump of 4 mN/m. Sidearms are numbered and measured along dendritic arms from the center of the domain up to the tip. Right side branches (filled symbols) and left side branches (open symbols).

experiment ($T = 22.4$ °C), after a pressure jump of 4 mN/m. Although, the side branches at the right and left sides are at different positions, both are disposed in a periodic way. The relation is almost linear; the linear correlation fitting coefficient is greater than 0.9 for each dendritic leg. For the experiment in Figure 9, the average distance between side branches is 5.9 ± 1.2 μm, and the average ratio of this periodicity and the measured tip radius for each dendrite leg is 3.8 ± 0.5. This number is similar to the quasi-2D dendrites obtained in NH_4-Br.[69]

We estimated the growth velocity of monolayer domains. One estimate comes from the jump experiments made on DODA presented above; another one comes from the ES monolayer compressed at high velocity. It is important to recall that we cannot in general observe a specific domain, since the monolayer is moving and our field of view is fixed; this is the case for S_1 DODA domains. Here, on electronic images coming from BAM, with the Image J software, we circumscribed domains with ellipses, which have to touch at least four out of six arms. Then, we plotted the ellipsis long axis versus time after the pressure jumps (results with ellipsis small axes are essentially the same). Growth velocities are between $0.08-0.13$ μm/s. For the case of ES compressed at high velocities (80 cm²/min), we measured tip-to-tip distances from opposite domain legs (passing through the domain center) from the video images as a function of time. We limited our measurements to those legs that were aligned. In this particular case, we could follow the growth of individual domains versus time. Our estimate, on average, for the domain growth velocity is 10.9 μm/s. However, there are examples of domains growing at velocities as low as 6.5 μm/s or as rapid 17.3 μm/s as well as domains with opposite legs with each one growing at a different velocity.

C. Doublons and AFM Observations of Transferred Monolayers. Figure 10 presents some examples of doublons formed after a small pressure jump in LMs. Although they are astonishing, they are not as large and well formed as in other systems presented in the literature;[45] probably, this is due to the lack of a more refined growth control in typical setups developed for monolayers. In our case, as growth proceeds, the channel becomes, in general, wider.

In Figure 11, we present phase lag AFM images coming from monolayers made of DODA, LB transferred on mica, at different stages of the domain growth. Here, we never observed well-developed dendrites as with direct observations of the mono-layer, because they are metastable structures, and during the

Figure 10. Doublons formed in Langmuir monolayers: (upper and middle panels) DODA, $T = 23.8$ °C, $\Pi = 5$ mN/m. The horizontal full width is 220 μm for each individual image. (lower panel) ethyl palmitate, $T = 20.3$ °C, $\Pi = 6$ mN/m. The horizontal full width is 430 μm for each individual image.

LB transfer, they probably transform into stabler domains. Thus, depending on the specific details of the LB transfer, we found structures going from thick deformed dendritic domains to nearly round domains. However, we never noticed structures different from those observed with BAM, and some interesting features can be observed. Figure 11a and c shows narrow channels going along a domain leg, typical of doublons. Figure 11b shows a thick domain with a tip-splitting leg, and Figure 11d shows a deformed thick dendritic domain on its way to reach its equilibrium shape. A feature interesting to mention is that many domains show a hole in the center. This could be seen in the AFM images (Figure 11a and b) and in some cases directly in the monolayer with BAM, in the later case, usually as Airy
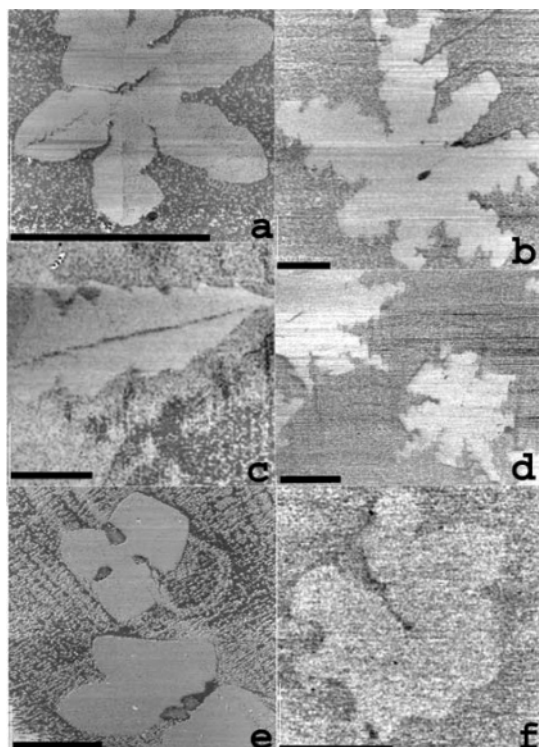
Pattern Formation and Morphology Evolution in LMs

J. Phys. Chem. B, Vol. 110, No. 10, 2006 **4831**

Figure 11. AFM images (phase lag) of LB transferred DODA monolayers on mica. Temperatures and pressure of LB transferring: (a) $T = 25.6$ °C, $\Pi = 6$ mN/m; (b) $T = 24.9$ °C, $\Pi = 8.5$ mN/m; (c) $T = 24.0$ °C, $\Pi = 5.0$ mN/m; (d) $T = 25.5$ °C, $\Pi = 7.0$ mN/m; (e) $T = 24.0$ °C, $\Pi = 5.0$ mN/m; (f) $T = 25.5$ °C, $\Pi = 7.0$ mN/m (the black line represents 10 μm).

Figure 12. BAM images showing the remnants of early doublons (channels or fjords), at very late stages of domain growth in the DODA monolayer: (a) $T = 23.9$ °C, $\Pi = 5.0$ mN/m, 5 min after pressure jump; next images at $T = 24.6$ °C, $\Pi = 1$ mN/m, time after pressure jump: (b) 100 min; (c) 6 h 10 min; (d) 6 h 12 min. The horizontal full width is 430 μm for each individual image.

rings due to diffraction. Figures 4d and 5a show small brilliant spots at the center of domains caused by the central peak of an Airy pattern.[70] We also noticed, after analyzing many BAM images and AFM images of transferred monolayers that doublons are very persistent, in the sense that although they become deformed during growth, it is very easy to recognize where it was a doublon in previous stages of domain evolution (Figure 11d−f). Usually, doublon remnants look like channels that start almost in the domain center and become wider away from the center (fjord). The BAM images in Figure 12 show remnants of early doublons at very late stages of domain growth in the DODA monolayer. In Figure 12a, doublons are easily observed in big seaweed domains in a stage where Ostwald ripening is present, that is, large and small domains, where the larger ones grow at the expense of the smaller ones. Figure 12b−d shows examples of domains at a long time after they were formed. Here, the channel starting at the center of the domain that becomes wider away from the center is easily observed, as well as different shades of gray due to the rotation of c-director. Domains with similar textures (six-segment star defects) and channels have been observed in chiral phospholipid dimyristoylphosphatidylethanolamine (DMPE) monolayers.[71]

Figure 13 shows the AFM height image version of Figure 11a (DODA monolayer) as well as a vertical cross section along the line crossing the image. In particular, here, we can observe the channel of the doublon (right A marker). On average, the height difference between the domain plateau and the LE phase level is ∼0.85 nm, due to the different tail tilting between the S_1 and LE phases in this monolayer.

D. Instability of the Circular Shape. In this section, we present results for experiments addressed to study the way in which the circular shape of growth for liquid condensed or solid domains becomes unstable; that is, we study the onset of the
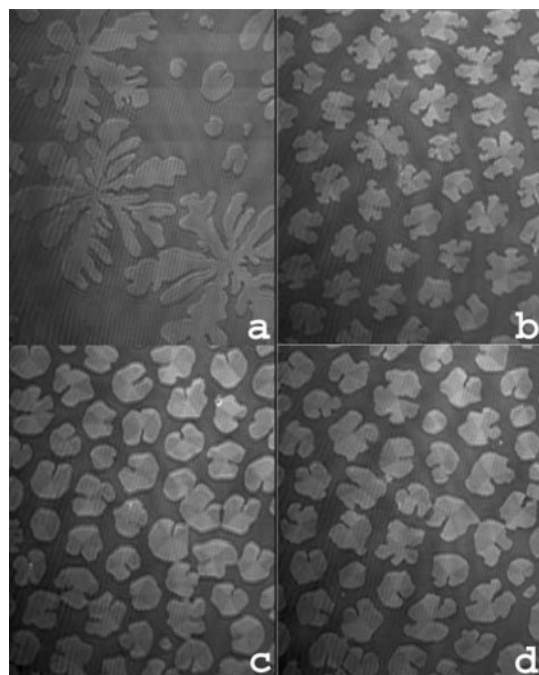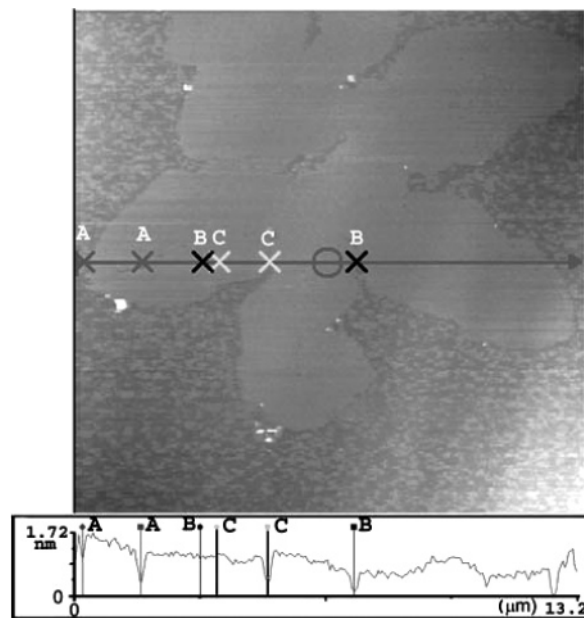

Figure 13. AFM height image version of Figure 11a (DODA monolayer) as well as a vertical cross section along the line crossing the image. The doublon channel is shown by the right A marker. S_1-LE height difference: C markers 0.66 nm, B markers: 0.90 nm.

instability. For this case, we used monolayers made of ES and of EP whose relaxation times are short. In these experiments, the monolayers were compressed gently up to the LE/L′$_2$ phase transition,[3] where round domains could be clearly observed with BAM; they were allowed to relax for ∼5 min. Then, we made a sudden compression of the monolayer that produced a lateral pressure jump. If the pressure jump is small (∼1 mN/m), the 1D circular interface deforms with a long wavelength undulation (see Figure 14). If pressure jumps are a little bit larger
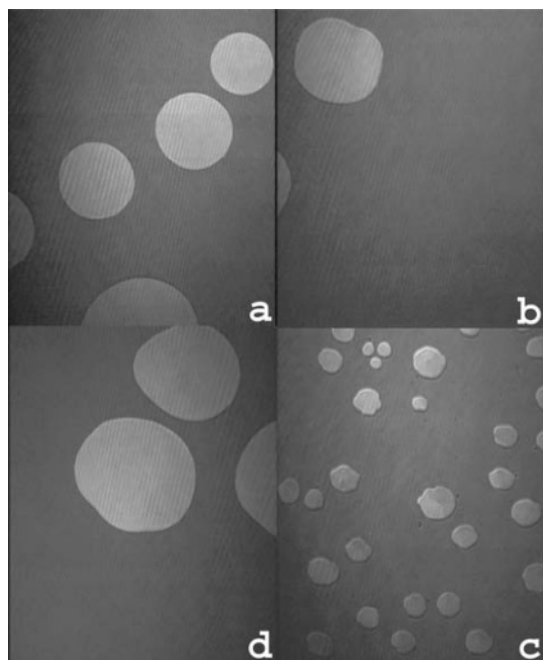
Figure 14. L$'_2$ domains of ethyl palmitate: (a) before the pressure jump, $T = 20.4$ °C, $\Pi = 5$ mN/m; (b and c) $T = 20.4$ °C, $\Pi = 6$ mN/m, after a jump of $\Delta\Pi = 1$ mN/m. L$'_2$ domains of ethyl stearate: (d) $T = 32$ °C, $\Pi = 5.5$ mN/m, after a jump of $\Delta\Pi = 1$ mN/m after a small lateral pressure jump. In both cases, the interface started to deform as an undulation of long wavelength. The horizontal full width is 430 μm.

($\sim$2 mN/m), an instability starts to develop at the circular interface. Structures similar to small fingers appear and grow at the interface line (see Figure 15). These fingers are clearly similar to the fingers found in several free-boundary problems, where it is possible to find spherical shape-preserving modes of growth and modes that become unstable.[20] As an example, in Figure 15, we present images of growing fingers from round domains of EP at the LE/L$'_2$ phase transition after a lateral pressure jump. Since we are able to observe the early stages of the destabilization, we report frequency histograms of distances, λ, between fingers. This distance was actually measured as the distance between neighboring valleys that have a finger between them (valley-to-valley distance). These values were obtained using the Image J software on our electronic BAM images. The histograms show a maximum at the most frequent value of λ. This implies that there is a wavelength that grows faster than the others, indicating that the competition between stabilizing and destabilizing effects leads to dynamics in which some modes grow, some modes decay, and there is a mode that grows faster than others modes, which determines the characteristic length of the pattern at short times. This is consistent with typical dispersion relations of classical free-boundary problems, for which the growth ratio at short times is a function of wave-number. They present a region of unstable modes with a maximum that corresponds to the fastest growing mode and a region of stable modes. In our experiments, no specific dependence on the domain radius was obtained. It is easy to observe with BAM how the fingertips start to bulge and continue their growth through tip splitting; this can be observed in some examples of Figure 14

E. Nonequilibrim Growth Morphologies in Langmuir Monolayers, Why? As mentioned in the Introduction, in LMs made of a single component, the problem of nonequilibrium growth morphologies is unclear. In 3D solidification from an
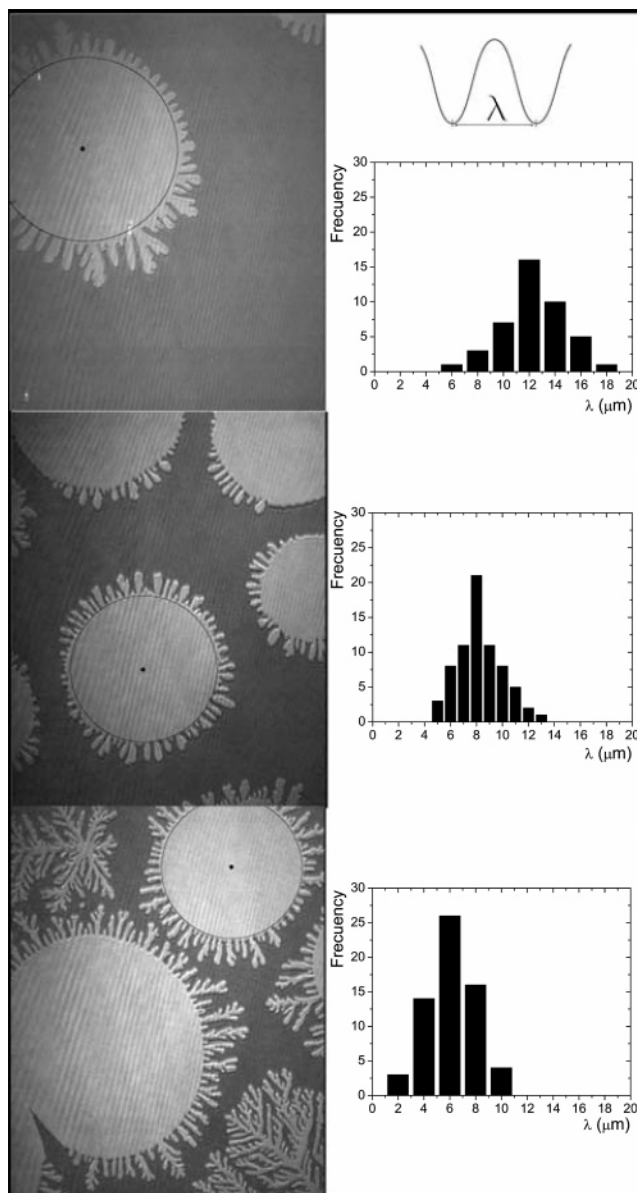

Figure 15. Growing fingers from round domains of ethyl palmitate at the LE/L$'_2$ phase transition after a small lateral pressure jump, as well as frequency charts vs repeat distance, λ, for the domains marked with a circle and a center, showing how many fingers are found at λ (radii for the worked domains: upper panel, 125.3 μm; medium panel, 100.4 μm; lower panel, 95.2 μm).

undercooled melt, interface propagation is limited because the latent heat released during the phase transformation has to be diffused away from the interface before further advancement can take place. This is not the case for LMs, because they rest on a large body of water that acts as an isothermal reservoir absorbing the heat released during phase transition. Therefore, a question arises: Why do we observe the nonequilibrium growth morphologies as described above? In this section, we present a possible explanation based on a model described below.

One characteristic that makes first-order phase transition between LE and condensed phases in monolayers different from their 3D analogues is that in monolayers the involved phases have a large density difference, of the order of 50%. As a result, domain growth will necessarily give rise to a density profile in the domain neighborhood. Therefore, mass diffusion must be a key variable to understand domain growth in LMs. In a model

developed by Bruinsma and collaborators,[68] they proposed a hydrodynamic mechanism based on Marangoni flow to describe growth instabilities and predicted some flow patterns both for the subphase and for the monolayer. Another possibility, not yet explored, could be to consider that, close to the melting point, diffusion could be dominant over convection flow due to the proper dynamics in 2D, where, as discussed by Zippelius, Halperin, and Nelson,[72] it seems to be a hexatic phase, which presents continuous dislocations and disclination-unbinding transitions.

Let us consider here a LM with two coexisting phases in thermodynamic equilibrium. Here, we will represent by LE the liquid expanded phase and by LC any condensed phase with a long-range or quasi-long-range order in some order parameter. We denote by μ the chemical potential of amphiphile molecules. This one is the same for both phases when the interface is flat or when the interface curvature is negligible; let us denote it by μ_o. ρ_l and ρ_s are the amphiphile densities for the LE and LC phases, respectively. If we impose a small, but abrupt, decrease in the total area occupied by the LM, as in the experiments described above, a transient increase in surface pressure ensues. Far from the LE/LC line boundary, both the amphiphile density and chemical potential in the LE phase increase by the amounts $\delta\rho$ and $\delta\mu$, respectively. The chemical potential, μ_0, and the density, ρ_s, in the LC phase change only by a negligible amount. For sufficiently low levels of supersaturation, that is, for sufficiently small values of $\delta\rho$ and $\delta\mu$, we can bring into play the condition of local thermodynamic equilibrium. Under these conditions, we reach a stationary state, where the chemical potential is a continuous function of position, and it must be equal on both sides of the LE/LC flat line boundary. Away from this LE/LC line boundary, μ increases monotonically until it reaches a value of $\mu_\infty = \mu_0 + \delta\mu$ at the monolayer boundary. The chemical potential gradient in the LE phase is the thermodynamic force that drives amphiphile molecules toward the LE/LC line boundary. Concomitant with the chemical potential, density increases monotonically from the line boundary until it reaches the asymptotic value $\rho_\infty = \rho_0 + \delta\rho$. Now, let us consider the case where the LC domains have a radius, R, to bring into play at the line interface the Gibbs−Thomson equation:

$$\mu(\text{interface}) - \mu_0(T) = -\frac{\tau}{\Delta\rho}\kappa \tag{1}$$

where κ is the local curvature, $\Delta\rho$ is the equilibrium density difference between the LE and LC phases at the temperature, T, and τ is the line tension. We also consider that the subphase has an infinite depth in the z-direction and it is also infinite, as the monolayer, in the perpendicular directions, $\perp$, that is, the plane where the monolayer rests. Now, consider that the monolayer is mainly in a LE phase coexisting with a few LC domains at temperature T, in a stationary state. Therefore, the density profile in the monolayer is the result of a mass balance in the thermodynamic force that drives amphiphile molecules toward the LE/LC line boundary:

$$D\nabla_\perp^2\mu = \frac{\partial}{\partial t}\mu \tag{2}$$

where D denotes the diffusion coefficient in the LE phase; the $\nabla_\perp$ operator applies only to the in-plane coordinates. There will be a similar equation with D' denoting the corresponding diffusion coefficient for the LC phase. It is important to mention that eq 2 can be obtained from hydrodynamic arguments, when

the surface viscous losses are dominant; however, this approach has some shortcomings that have to be solved; this work is in progress.

In the stationary state, eq 2 gives

$$\nabla_\perp^2\mu = 0 \tag{3}$$

Thus, the equation governing the monolayer in this regime is Laplace's equation in the chemical potential. This equation has to be solved with two boundary conditions at the interface given by the Gibbs−Thomson boundary condition, eq 1, and by the conservation boundary condition:

$$v_n = \frac{M}{\Delta\rho}[\beta(\nabla_\perp\mu)_s - (\nabla_\perp\mu)_l]\cdot\mathbf{n} \tag{4}$$

where v_n is the normal velocity to the line interface and $\beta = M'/M$ is the ratio of LC to LE mobilities, M' and M, respectively; the diffusion coefficient is $D = M(\partial\mu/\partial\rho)$.

It is important to note that eq 3, with the boundary conditions at the interface given by eqs 1 and 4, is similar to the equation used by Müller-Krumbhaar and collaborators[10−15] to analytically construct the kinetic phase diagram, if we would include in the Gibbs−Thomson equation a supersaturation parameter, Δ, and a capillary length with an anisotropy parameter, ϵ, that is, $d = d_0(1 - \epsilon \cos n\theta)$.[10−15] Here, d_0 is the so-called capillary length defined by $d_0 = \tau/(\Delta\rho)^2(\partial\mu/\partial\rho)$.[20] That is, if eq 1 would be written as

$$\frac{\mu(\text{interface}) - \mu_0(T)}{\Delta\rho\left(\frac{\partial\mu}{\partial\rho}\right)} = \Delta - d\kappa \tag{5}$$

The factors used here were included for an easy identification with the work of Müller-Krumbhaar and collaborators.[10−15] The diagram predicted by those authors has regions of different morphological structures and lines indicating transitions between such morphological structures. The control parameters are the degree of undercooling, Δ, and the strength of anisotropy, ϵ, in the solid phase. They could discriminate between compact structures and fractal structures as well as between structures with orientational order, such as dendritic structures, and structures without apparent orientational order, such as seaweed structures. Therefore, we consider that this is the underlying reason to have dendritic and seaweed structures in monolayers: The steady-state equation governing the monolayer is Laplace's equation in the chemical potential. The transitions between morphological structures must be related to moving the control parameters through the boundary lines along the morphological phase diagram. This deserves further investigation that is underway.

Stability Analysis. Finally, we consider revising the circular shape-preserving modes of growth and the way in which the circular shape becomes unstable. Consider first a circular domain. We will use eqs 3, 1, and 4 but with a dimensionless diffusion field,[20] $U = (\mu - \mu_o)/\Delta\rho(\partial\mu/\partial\rho)$. Let the radius of the circle be R_0, and let the supersaturation far away from the circle, R_∞, be Δ:

$$U(R_\infty) = -\Delta \tag{6}$$

In the quasi-stationary approximation, the diffusion field that

4834 *J. Phys. Chem. B, Vol. 110, No. 10, 2006*

Flores et al.

satisfies Laplace's equation everywhere in 2D can be written as

$$
U_o = \begin{cases} -\dfrac{d_o}{R_o} & r < R_o \\[2em] -\dfrac{d_o}{R_o} + \dfrac{\left[-\Delta + \dfrac{d_o}{R_o}\right]}{\ln\dfrac{R_\infty}{R_o}}\ln r/R_o & r > R_o \end{cases} \tag{7}
$$

Here, r is the radius measured from the center of the round domain and the boundary condition (1) has been imposed at $r = R_o$. The continuity condition (4) determines the growth rate:

$$
v_n = -\frac{D}{R_o}\frac{\left[-\Delta + \dfrac{d_o}{R_o}\right]}{\ln\dfrac{R_\infty}{R_o}} \tag{8}
$$

Now, let us consider the case of a slightly perturbed round domain, whose radius is given by the following expression:

$$
R = R_o + \delta_n \cos n\theta\, e^{\omega t} \tag{9}
$$

where δ_n is a small deformation amplitude. Thus, associated with the deformation, there is a diffusion field of the form

$$
U = \begin{cases} -\dfrac{d_o}{R_o} + b_n r^n \cos n\theta\, e^{\omega t} & r < R_o \\[2em] -\dfrac{d_o}{R_o} + \dfrac{\left[-\Delta + \dfrac{d_o}{R_o}\right]}{\ln\dfrac{R_\infty}{R_o}}\ln r/R_o + \dfrac{a_n}{r^n}\cos n\theta\, e^{\omega t} & r > R_o \end{cases} \tag{10}
$$

a_n and b_n can be calculated by evaluating (9) at $r = R$, in eq 1 through linearization. The curvature for the perturbed circle given by eq 9 can be evaluated using the general expression for a curve in a plane, $\mathbf{r}(t)$:

$$
\kappa = \frac{r''r'^2 - (\mathbf{r}'\cdot\mathbf{r}'')^2}{(r'^2)^3}
$$

The result to first order in δ_n/R_o is

$$
\kappa = \frac{1}{R_o}\left(1 + \frac{[n^2 - 1]}{R_o}\delta_n \cos n\theta\, e^{\omega t}\right) \tag{11}
$$

Therefore, the expressions for a_n and b_n are

$$
\frac{\delta_n}{R_o}\frac{\left[-\Delta + \dfrac{d_o}{R_o}\right]}{\ln\dfrac{R_\infty}{R_o}} + \frac{a_n}{R_o^{\,n}} = -\frac{d_o}{R_o^{\,2}}(n^2 - 1)\delta_n \tag{12}
$$

and

$$
b_n = -\frac{d_o}{R_o^{\,n+2}}(n^2 - 1)\delta_n \tag{13}
$$

In a similar way, using the continuity condition (4) and making the same kind of linearization as before, we obtain

$$
\omega\delta_n = D\beta n b_n R_o^{\,n-1} + \frac{D\delta_n\left[-\Delta + \dfrac{d_o}{R_o}\right]}{R_o^{\,2}\ln\dfrac{R_\infty}{R_o}} + \frac{Dna_n}{R_o^{\,n+1}} \tag{14}
$$

Equation 14 can be rewritten using eqs 12 and 13 to obtain the amplification rate or the dispersion relation for our problem:

$$
\omega_n = [n - 1]\frac{v_R}{R_o}\left[1 - \frac{n(n + 1)Dd_o[\beta + 1]}{v_R R_o^{\,2}}\right] \tag{15}
$$

The right-hand side of this formula contains two parts: a positive destabilizing term, which is proportional to the velocity, and a negative stabilizing term, which contains the surface tension. This result is in agreement with classical dispersion relations and could explain why, in the experiments presented above, addressed to study the manner in which the circular shape becomes unstable, just the fingers with dominant periodicities grow.

Another kind of shape instability has been studied in lipid monolayers, where transitions from circular shapes to domains with shapes of lower symmetry are driven by long-range dipole−dipole electrostatic repulsions and are opposed by line tension that stabilizes circular shape.[73,74] Shape distortions with a magnitude a fraction of the radius occur over a period of minutes. The dynamics of these shape transitions is determined by a competition between a driving force (electrostatic−line tension imbalance) within the monolayer and the viscous drag of the aqueous subphase. The rate of shape change at short times for domains has been calculated.[73,74] In a particular case, it was obtained that monolayers follow Darcy's equation (in a shallow aqueous subphase),[74] which with suitable boundary conditions could produce patterns as in the Saffman−Taylor instability. Although in many features these shape instabilities are similar to those presented in this paper, in our case as mentioned before, the interface becomes unstable because of the competition between a chemical potential gradient, determined by the imposed supersaturation that destabilizes the interface, and line tension that stabilizes the interface.

4. Conclusions

We have showed that, in monolayers, domain growth of condensed phases from a metastable phase presents several stages. Domain growth starts, and depending on the supersaturation level, the shape becomes unstable. Some unstable modes grow faster and structures evolve through tip-splitting dynamics. At high supersaturation levels, there is a morphological transition. Domains start to grow with needle tips, which show as growth proceeds side branching. We observed doublons and how they persist in a deformed way at late stages of domain growth. In addition, we showed how the instability starts at round domains when a small lateral pressure jump is applied to the monolayer; frequency histograms for the distance between neighboring fingers were presented, which are consistent with classical linear stability results for free-boundary problems. Finally, we presented a model for monolayer growth, which can be related to the theory of dynamic phase transitions developed by Müller-Krumbhaar and collaborators,[10−15] where morphological structures and morphological transitions can be obtained. This model also provides a dispersion relation that

Pattern Formation and Morphology Evolution in LMs

J. Phys. Chem. B, Vol. 110, No. 10, 2006 **4835**

could explain which modes of growth preserve the circular shape and which ones become unstable.

Supporting Information Available: Film obtained with Brewster angle microscopy showing a Langmuir monolayer of ethyl stearate where L'_2 is phase growing into the LE phase at relatively high speed. The monolayer was compressed at 80 cm^2/min, at $T = 32$ °C, and the subphase is water/glycerol (10 vol %). The horizontal full width is 430 μm. The elapsed time between the first image and the last image is 7.5 s. This material is available free of charge via the Internet at http://pubs.acs.org.

References and Notes

(1) Stenhagen, E. In *Determination of Organic Structure by Physical Methods*; Braude, E. A., Nachord, F. C., Eds.; Academic Press: New York, 1955.

(2) Lundquist, M. *Prog. Chem. Fats Other Lipids* **1978**, *16*, 101.

(3) Lundquist, M. *Chem. Scr.* **1971**, *1*, 197.

(4) Andelman, D.; Brochard, F.; Knobler, C. M.; Rondelez, F. In *Micelles, Membranes, Microemulsions,* and Monolayers; Gelbart, W. M., Ben-Sahul, A., Roux, D., Eds.; Springer, New York, 1994.

(5) Kaganer, V. M.; Möhwald, H.; Dutta, P. *Rev. Mod. Phys.* **1999**, *71*, 779.

(6) Als-Nielsen, J.; Jacquemain, D.; Kjaer, K.; Leveiller, F.; Lahav, M.; Leiserowitz, L. *Phys. Rep.* **1994**, *246*, 251.

(7) Knobler, C. M. In *Advances in Chemical Physics*; Prigogine, I., Rice, S. A., Eds.; Wiley: New York, 1990; Vol. LXXVII, p 397.

(8) Höning, D.; Möbius, D. *J. Phys. Chem.* **1991**, *95*, 4590.

(9) Henon, S.; Meunier, J. *Rev. Sci. Instrum.* **1991**, *62*, 936.

(10) Brener, E.; Müller-Krumbhaar, H.; Temkin, D. *Europhys. Lett.* **1992**, *17*, 535.

(11) Brener, E.; Kassner, K.; Müller-Krumbhaar, H.; Temkin, D. *Int. J. Mod. Phys. C.* **1992**, *3*, 825.

(12) Brener, E.; Müller-Krumbhaar, H.; Temkin, D. *Phys. Rev. E* **1996**, *54*, 2714.

(13) Brener, E.; Müller-Krumbhaar, H.; Temkin, D.; Abel, T. *Physica A* **1998**, *249*, 73.

(14) Ihle, T.; Müller-Krumbhaar, H. *Phys. Rev. Lett.* **1993**, *70*, 3083.

(15) Ihle, T.; Müller-Krumbhaar, H. *Phys. Rev. E* **1994**, *49*, 2972.

(16) Ben-Jacob, E. *Contemp. Phys.* **1993**, *34*, 247.

(17) Ivantsov, G. P. *Dokl. Akad. Nauk. SSSR* **1947**, *58*, 567.

(18) Glicksman, M. E.; Schaefer, R. J.; Ayers, J. D. *Metall. Mater. Trans. A* **1976**, *7*, 1747.

(19) Mullins, W. W.; Sekerka, F. F. *J. Appl. Phys.* **1964**, *35*, 444.

(20) Langer, J. S. *Rev. Mod. Phys.* **1980**, *52*, 1.

(21) Ben Amar, M.; Pomeau, Y. *Europhys. Lett.* **1986**, *2*, 307.

(22) Langer, J. S. *Science* **1989**, *243*, 1150.

(23) Brower, R. C.; Kessler, D. A.; Koplik, J.; Levine, H. *Phys. Rev. Lett.* **1983**, *51*, 1111.

(24) Ben-Jacob, E.; Goldenfeld, N.; Langer, J. S.; Schön, G. *Phys. Rev. Lett.* **1983**, *51*, 1930.

(25) Gonzalez-Cinca, R.; Folch, R.; Benitez, R.; Ramirez-Piscina, L.; Casademunt, J.; Hernandez-Machado, A. In *Advances in Condensed Matter and Statistical Physics*; Korutcheva, E., Cuerno, R., Eds.; Nova Science Publishers: New York, 2004.

(26) Kobayashi, R. *Physica D* **1993**, *63*, 410.

(27) Karma, A.; Rappel, W. J. *Phys. Rev. E* **1996**, *53*, 3017.

(28) Karma, A.; Rappel, W. J. *Phys. Rev. E* **1998**, *57*, 4323.

(29) Provatas, N.; Goldenfeld, N.; Dantzig, J. *Phys. Rev. Lett.* **1998**, *80*, 3308.

(30) Provatas, N.; Wang, Q.; Haataja, M.; Grant, M. *Phys. Rev. Lett.* **2003**, *91*, 155502.

(31) Gonzalez-Cinca, R.; Ramirez-Piscina, L.; Casademunt, J.; Hernandez-Machado, A. *Phys. Rev. E* **2001**, *63*, 51602.

(32) Gonzalez-Cinca, R.; Couder, Y.; Hernandez-Machado, A. *Phys. Rev. E* **2005**, *71*, 51601.

(33) Witten, T. A.; Sander, L. M. *Phys. Rev. B* **1983**, *27*, 5686.

(34) Witten, T. A.; Sander, L. M. *Phys. Rev. Lett.* **1981**, *47*, 1400.

(35) Uwaha, M.; Saito, Y. *Phys. Rev. A* **1989**, *40*, 4716.

(36) Liu, F.; Goldenfeld, N. D. *Phys. Rev. A* **1990**, *42*, 895.

(37) Vicsek, T. *Phys. Rev. Lett.* **1984**, *24*, 2281.

(38) Vicsek, T. *Phys. Rev. A* **1985**, *32*, 3084.

(39) Sander, L. M. *Contemp. Phys.* **2000**, *41*, 203.

(40) Paterson, L. *Phys. Rev. Lett.* **1984**, *52*, 1621.

(41) Sander, L. M. *Nature* **1986**, *322*, 789.

(42) Nittmann, J.; Stanley H. E. In *Fractals and Disordered systems*; Bunde, A., Havlin, S., Eds.; Springer Verlag: Berlin, 1991.

(43) Barra, F.; Davidovitch, B.; Levermann, A.; Procaccia, I. *Phys. Rev. Lett.* **2001**, *87*, 134501.

(44) Hentschel, H. G. E.; Levermann, A.; Procaccia, I. *Phys. Rev. E* **2002**, *66*, 16308.

(45) Akamatsu, A.; Faivre, G.; Ihle T. *Phys. Rev. E* **1995**, *51*, 4751.

(46) Bisang U.; Bilgram, J. H. *Phys. Rev. E* **1996**, *54*, 5309.

(47) Utter, B.; Ragnarsson, R.; Bodenschatz, E. *Phys. Rev. Lett.* **2001**, *20*, 4604.

(48) Stalder, I.; Bilgram, J. H. *Europhys. Lett.* **2001**, *56*, 829.

(49) Singer, H. M.; Bilgram, J. H. *Phys. Rev. E* **2004**, *70*, 31601.

(50) Taguchi, K.; Miyaji, H.; Izumi, K.; Hoshino, A.; Miyamoto, Y.; Kokawa, R. *Polymer* **2001**, *42*, 7443.

(51) Ferreiro, V.; Douglas, J. F.; Warren, J.; Karim, A. *Phys. Rev. E* **2002**, *65*, 51606.

(52) Keller, D. J.; Korb, J. P.; McConnell, H. M. *J. Phys. Chem.* **1987**, *91*, 6417.

(53) McConnell, H. M.; Moy, V. T. *J. Phys. Chem.* **1988**, *92*, 4520.

(54) McConnell, H. M.; De Koker, R. *Langmuir* **1996**, *12*, 4897.

(55) Seul, M.; Andelman, D. *Science* **1995**, *267*, 476.

(56) Miller, A.; Möhwald, H. *J. Chem. Phys.* **1987**, *86*, 4258.

(57) Akamatsu, S.; Bouloussa, O.; To, K.; Rondelez, F. *Phys. Rev. A* **1992**, *46*, 4505.

(58) Weidemann, G.; Vollhardt, D. *Langmuir* **1997**, *13*, 1623.

(59) Gehlert, U.: Vollhardt, D. *Langmir* **1997**, *13*, 277.

(60) Imura, K.; Yamauchi, Y.; Tsuchiya Y.; Kato, T.; Suzuki, M. *Langmuir* **2001**, *17*, 4602.

(61) Flores A.; Ize, P.; Ramos, S.; Castillo, R. *J. Chem. Phys.* **2003**, *119*, 5644.

(62) Nandi, N.; Vollhardt, D. *Chem. Rev.* **2003**, *103*, 4033.

(63) Weidemann, G.; Vollhardt, D. *Biophys. J.* **1996**, *70*, 2758.

(64) Vollhardt, D.; Emrich, G.; Gutberlet, T.; Fuhrhop, J.-H. *Langmuir* **1996**, *12*, 5659.

(65) Vollhardt, D.; Gutberlet, T.; Emrich, G.; Fuhrhop, J.-H. *Langmuir* **1995**, *11*, 2661.

(66) Hoffmann, F.; Stine, K. J.; Hühnerfuss, H. *J. Phys. Chem. B* **2005**, *109*, 240.

(67) Valance, A.; Misbah, C. *Phys. Rev. E* **1997**, *55*, 5564.

(68) Bruinsma, R.; Rondelez, F.; Levine, A. *Eur. Phys. J. E* **2001**, *6*, 191.

(69) Dougherty, A.; Kaplan, P. D.; Gollub, J. P. *Phys. Rev. Lett.* **1987**, *58*, 1652.

(70) Galvan-Miyoshi, J.; Ramos, S.; Ruiz-García J.; Castillo R. *J. Chem. Phys.* **2001**, *115*, 8178.

(71) Ignes-Mullol, J.; Claret, J.; Sagues, F. *J. Phys. Chem. B* **2004**, *108*, 612.

(72) Zippelius, A.; Halperin, B. I.; Nelson, D. R. *Phys. Rev. B* **1980**, *22*, 2514.

(73) Stone, H. A.; McConnell, H. M. *Proc. R. Soc. London, Ser. A* **1995**, *448*, 97.

(74) Stone, H. A.; McConnell, H. M. *J. Phys. Chem.* **1995**, *99*, 13505.